Beamforming Optimization for Wireless Network Aided by Intelligent Reflecting Surface With Discrete Phase Shifts

Qingqing Wu, *Member, IEEE*, and Rui Zhang, *Fellow, IEEE*

***Abstract*— Intelligent reflecting surface (IRS) is a cost-effective solution for achieving high spectrum and energy efficiency in future wireless networks by leveraging massive low-cost passive elements that are able to reflect the signals with adjustable phase shifts. Prior works on IRS mainly consider continuous phase shifts at reflecting elements, which are practically difficult to implement due to the hardware limitation. In contrast, we study in this paper an IRS-aided wireless network, where an IRS with only a finite number of phase shifts at each element is deployed to assist in the communication from a multi-antenna access point (AP) to multiple single-antenna users. We aim to minimize the transmit power at the AP by jointly optimizing the continuous transmit precoding at the AP and the discrete reflect phase shifts at the IRS, subject to a given set of minimum signal-to-interference-plus-noise ratio (SINR) constraints at the user receivers. The considered problem is shown to be a mixed-integer non-linear program (MINLP) and thus is difficult to solve in general. To tackle this problem, we first study the single-user case with one user assisted by the IRS and propose both optimal and suboptimal algorithms for solving it. Besides, we analytically show that as compared to the ideal case with continuous phase shifts, the IRS with discrete phase shifts achieves the same squared power gain in terms of asymptotically large number of reflecting elements, while a constant proportional power loss is incurred that depends only on the number of phase-shift levels. The proposed designs for the single-user case are also extended to the general setup with multiple users among which some are aided by the IRS. Simulation results verify our performance analysis as well as the effectiveness of our proposed designs as compared to various benchmark schemes.**

***Index Terms*— Intelligent reflecting surface, joint active and passive beamforming design, discrete phase shifts optimization.**

I. Introduction

ALTHOUGH massive multiple-input multiple-output (MIMO) technology has significantly improved the spectrum efficiency of wireless communication systems, the required high complexity, high energy consumption, and high hardware cost are still the main hindrances to its implementation in practice [2]–[5]. Recently, intelligent reflecting surface (IRS) has been proposed as a new and cost-effective solution for potentially achieving high spectrum and energy efficiency for wireless communications via only low-cost reflecting elements [6], [7]. An IRS is generally composed of a large number of passive elements each being able to reflect the incident signal with an adjustable phase shift. By smartly tuning the phase shifts of all elements adaptively according to the dynamic wireless channels, the signals reflected by an IRS can add constructively or destructively with those non-reflected by it at a nearby user receiver to boost the desired signal power and/or suppress the co-channel interference, thus significantly enhancing the communication performance without the need of deploying additional active base stations (BSs) or relays. In addition, without employing any transmit radio frequency (RF) chains, IRSs usually have much smaller signal coverage than active BSs/relays, which makes it easier to practically deploy them without interfering each other. Moreover, from the implementation perspective, IRSs possess appealing features such as low profile and lightweight, thus can be easily mounted on walls or ceilings of buildings, while integrating them into the existing cellular and WiFi systems does not require any change in the hardware at the BSs/access points (APs) as well as user terminals. As compared to existing wireless technologies based on active elements/RF chains such as MIMO relay and massive MIMO, it has been shown in [6], [7] that IRS with only passive reflecting elements can potentially yield superior performance scaling with the increasing number of elements, but at substantially reduced hardware and energy costs. It is worth noting that there have been other terminologies similar to IRS proposed in the literature, such as intelligent wall [8], passive intelligent mirror [9], [10], smart reflect-array [11], and reconfigurable metasurface [12], among others.

IRS-aided wireless communications have drawn significant research attention recently (see, e.g. [6], [7], [13]–[18]). Specifically, for the IRS-aided wireless system with a single user, it was firstly shown in [7], [13] that the IRS is capable of creating a "signal hot spot" in its vicinity via joint active beamforming at the BS/AP and passive beamforming at the IRS. In particular, an asymptotic receive signal power or signal-to-noise ratio (SNR) gain in the order of $\mathcal{O}(N^2)$,

Manuscript received June 7, 2019; revised October 10, 2019 and December 2, 2019; accepted December 5, 2019. Date of publication December 10, 2019; date of current version March 18, 2020. This article has been presented in part by the IEEE International Conference on Acoustics, Speech, and Signal Processing [1]. The associate editor coordinating the review of this article and approving it for publication was E. Björnson. *(Corresponding author: Qingqing Wu.)*

The authors are with the Department of Electrical and Computer Engineering, National University of Singapore, Singapore 119077 (e-mail: elewuqq@nus.edu.sg; elezhang@nus.edu.sg).

Color versions of one or more of the figures in this article are available online at http://ieeexplore.ieee.org.

Digital Object Identifier 10.1109/TCOMM.2019.2958916

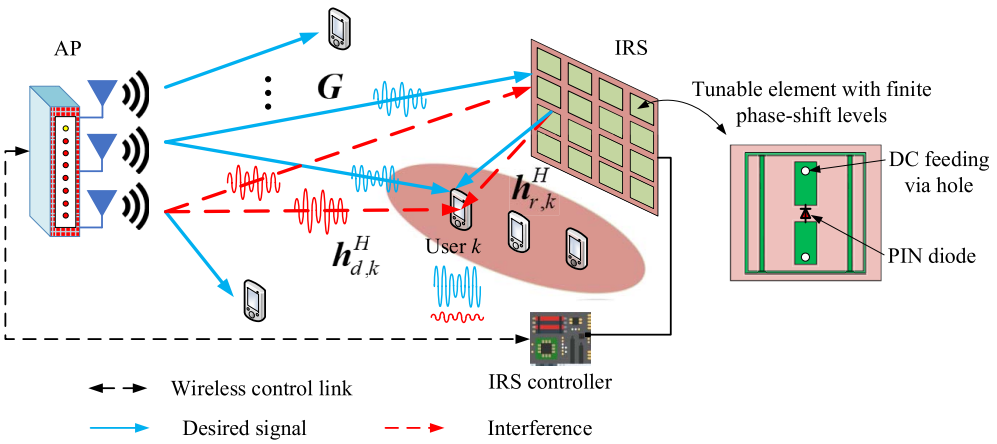

Fig. 1. An IRS-aided multiuser wireless communication system.

with N denoting the number of reflecting elements at the IRS, was shown when N is sufficiently large in practice. Such a *squared power/SNR gain* is larger than that of massive MIMO, i.e., $\mathcal{O}(N)$ [3], due to the fact that the IRS combines the functionalities of both receive and transmit arrays for energy harvesting and reflect beamforming, respectively, thus doubling the gain as compared to massive MIMO with a constant total transmit power regardless of N. In addition, with conventional MIMO relays (even assuming their full-duplex operation with perfect self-interference cancellation), the SNR at the user receiver increases with the number of active antennas, N, only with $\mathcal{O}(N)$ due to the noise effect at the relay [7], which is also lower than $\mathcal{O}(N^2)$ of the IRS thanks to its full-duplex and noise-free signal reflection. An interesting comparison between the IRS-aided single-input single-output (SISO) system and the massive MIMO system is studied in [19]. Furthermore, for a general multiuser system aided by IRS as shown in Fig. 1, it was shown in [7] that besides enhancing the desired signal power/SNR at the user receiver, a virtually "interference-free" zone can also be established in the proximity of the IRS, by exploiting its spatial interference nulling/cancellation capability. In particular, a user near the IRS is able to tolerate more interference from the AP as compared to others outside the coverage region of the IRS. This thus provides more flexibility for designing the transmit precoding at the AP for such "outside" users and as a result improves the signal-to-interference-plus-noise ratio (SINR) performance of all users in the system. The joint active and passive beamforming design was also investigated in other system setups, e.g., physical layer security [17], [20]–[22], simultaneous wireless information and power transfer (SWIPT) [23]–[26], and non-orthogonal multiple access [27], [28].

The hardware implementation of IRS is based on the concept of "metasurface", which is made of two-dimensional (2D) metamaterial with high controllability [6], [12], [29]–[31]. By properly designing each element of the metasurface, including geometry shape (e.g., square or split-ring), size/dimension, orientation, etc., different phase shifts of the reflected signal can be resulted. However, for wireless communication applications, it is more desirable to adjust the phase shifts by the IRS in real time to cater for time-varying wireless channels arising from the user mobility. This can be realized by leveraging electronic devices such as positive-intrinsic-negative (PIN) diodes, micro-electromechanical system (MEMS) based switches, or field-effect transistors (FETs) [32]. In Fig. 1, we show one example of a tunable element's structure, in which a PIN diode is embedded in the center to achieve the binary phase shifting. Specifically, the PIN diode can be switched between "On" and "Off" states by controlling its biasing voltage via a direct-current (DC) feeding line, thereby generating a phase-shift difference of π in rad [6], [29]. Moreover, the switching frequency of the PIN diode can be up to 5 MHz [31], which makes the switching time negligible as compared to the typical wireless channel coherence time. In practice, different phase shifts at IRS's elements can be realized independently via setting the corresponding biasing voltages by using a smart IRS controller. Therefore, the main power consumption of IRS is due to the feeding circuit of the diode used to tune the elements (on the order of microwatts [30]), which is significantly lower than that by transmit RF chains of conventional active arrays [3], [33].

The existing works [7], [9], [10], [13]–[17], [34] on IRS-aided wireless communications are mainly based on the assumption of continuous phase shifts at its reflecting elements. However, in practice, this is difficult to realize since manufacturing each reflecting element with more levels of phase shifts incurs a higher cost, which may not be scalable as the number of elements for IRS is usually very large [35]. For example, to enable 16 levels of phase shifts, $\log_2 16 = 4$ PIN diodes need to be integrated to each element. This not only makes the element design more challenging due to its limited size, but also requires extra controlling pins at the IRS controller to control more PIN diodes. Although a single varactor diode can be used to achieve more than two phase shifts, it requires a wide range of biasing voltages. As such, for practical IRSs with a large number of elements, it is more cost-effective to implement only discrete phase shifts with a small number of control bits for each element, e.g., 1-bit for two-level (0 or π) phase shifts [1], [11], [29]. Note that such

limited discrete phase shifts inevitably cause misalignment of IRS-reflected and non-IRS-reflected signals at designated receivers and thus result in certain performance degradation, which needs to be investigated for practically deploying low-resolution IRSs in future wireless systems. Besides, it remains unknown whether the "squared power/SNR gain" revealed in [7] still holds for the case of IRS with discrete phase shifts, as well as how the resultant discrete-phase constraints impact the IRS's passive beamforming design jointly with the AP's active transmit precoding.

Motivated by the above, we study in this paper an IRS-aided multiuser wireless communication system shown in Fig. 1, where a multi-antenna AP serves multiple single-antenna users with the help of an IRS. In contrast to the continuous phase shifts assumed in [7], [9], [10], [13]–[17], [34], we consider the practical case where each element of the IRS has only a finite number of discrete phase shifts. We aim to minimize the transmit power required at the AP via jointly optimizing the active transmit precoder at the AP and passive reflect discrete phase shifts at the IRS, subject to a given set of SINR constraints at the user receivers. However, the transmit precoder and discrete phase shifts are intricately coupled in the SINR constraints, rendering the formulated optimization problem a mixed-integer non-linear program (MINLP) that is NP-hard and thus difficult to solve in general.

To tackle this new problem, we first consider the single user setup where there is only one active user served by a nearby IRS. By exploiting the structure of the simplified problem, we show that it can be transformed into an integer linear program (ILP), for which the globally optimal solution can be obtained by applying the branch-and-bound method. To reduce the computational complexity for the optimal solution, we further propose a low-complexity successive refinement algorithm where the optimal discrete phase shifts of different elements at the IRS are determined one by one in an iterative manner with those of the others being fixed. This algorithm is shown to achieve close-to-optimal performance. Moreover, we analytically show that when the number of reflecting elements at the IRS, N, increases, the power loss due to discrete phase shifts as compared to the ideal case with continuous phase shifts approaches a constant in dB that depends only on the number of phase-shift levels at each element, but regardless of N as $N \to \infty$. As a result, the asymptotic squared power gain of $\mathcal{O}(N^2)$ by the IRS shown in [13] with continuous phase shifts still holds with discrete phase shifts. Next, we extend the successive refinement algorithm to the general case with multiple users at arbitrary locations in the network, by considering the suboptimal zero-forcing (ZF) based linear precoding at the AP for low-complexity implementation. Numerical results are shown to validate our theoretical analysis and demonstrate the effectiveness of using IRS with practical discrete phase shifts to improve the performance of wireless networks as compared to the case without using IRS. Furthermore, it is shown that the proposed algorithms for joint AP precoding and IRS discrete phase shifts optimization outperform both the quantization-based and codebook-based schemes with IRS. Finally, we show that employing practical IRS with even finite-level low-cost phase shifters in wireless networks is able to achieve the same multiuser SINR performance as compared to the conventional large (massive) MIMO system without using the IRS, but instead using more active antennas at the AP, thus significantly reducing the system energy consumption as well as hardware cost.

The rest of this paper is organized as follows. Section II introduces the system model and the problem formulation for the IRS-aided wireless system with discrete phase shifts. In Sections III and IV, we propose both optimal and suboptimal algorithms to solve the optimization problems in single-user and multiuser cases, respectively. Section V presents numerical results to evaluate the performance of the proposed designs. Finally, this paper is concluded in Section VI.

Notations: Scalars are denoted by italic letters, vectors and matrices are denoted by bold-face lower-case and upper-case letters, respectively. $\mathbb{C}^{x\times y}$ denotes the space of $x \times y$ complex-valued matrices. For a complex-valued vector $\boldsymbol{x}$, $\|\boldsymbol{x}\|$ denotes its Euclidean norm, $\arg(\boldsymbol{x})$ denotes a vector with each entry being the phase of the corresponding entry in $\boldsymbol{x}$, and $\text{diag}(\boldsymbol{x})$ denotes a diagonal matrix with each diagonal entry being the corresponding entry in $\boldsymbol{x}$. The distribution of a circularly symmetric complex Gaussian (CSCG) random vector with mean vector $\boldsymbol{x}$ and covariance matrix $\boldsymbol{\Sigma}$ is denoted by $\mathcal{CN}(\boldsymbol{x}, \boldsymbol{\Sigma})$; and $\sim$ stands for "distributed as". For a square matrix $\boldsymbol{S}$, $\text{tr}(\boldsymbol{S})$ and $\boldsymbol{S}^{-1}$ denote its trace and inverse, respectively, while $\boldsymbol{S} \succeq \boldsymbol{0}$ means that $\boldsymbol{S}$ is positive semi-definite. For any general matrix $\boldsymbol{A}$, $\boldsymbol{A}^H$, $\text{rank}(\boldsymbol{A})$, and $\boldsymbol{A}(i,j)$ denote its conjugate transpose, rank, and (i,j)th entry, respectively. $\boldsymbol{I}_M$ denotes an identity matrix with size $M \times M$. $\mathbb{E}(\cdot)$ denotes the statistical expectation. $\text{Re}\{\cdot\}$ denotes the real part of a complex number. For a set $\mathcal{K}$, $|\mathcal{K}|$ denotes its cardinality.

II. System Model and Problem Formulation

A. System Model

As shown in Fig. 1, we consider a multiuser multiple-input single-output (MISO) wireless system where an IRS composed of N reflecting elements is deployed to assist in the downlink communication from an AP with M antennas to K single-antenna users over a given frequency band. The sets of reflecting elements and users are denoted by $\mathcal{N}$ and $\mathcal{K}$, respectively, where $|\mathcal{N}| = N$ and $|\mathcal{K}| = K$. While this paper focuses on the downlink communication, the results are extendable to the uplink communication as well by exploiting the uplink-downlink channel reciprocity. In practice, each IRS is usually attached with a smart controller that communicates with the AP via a separate wireless link for coordinating transmission and exchanging information on e.g. channel knowledge, and controls the phase shifts of all reflecting elements in real time [6]. Due to the substantial path loss, we consider only the signal reflection by the IRS for the first time and ignore the signals that are reflected by it two or more times. In addition, the quasi-static flat-fading model is assumed for all channels. To characterize the optimal performance of the IRS-aided wireless system with discrete phase shifts, it is assumed that

the channel state information (CSI) of all channels involved is perfectly known at the AP in each channel coherence time, based on the various channel acquisition methods discussed in [6].[1]

According to [6] and under the assumption of an ideal signal refection model by ignoring the hardware imperfections such as non-linearity and noise, the reflected signal by the nth element of the IRS, denoted by $\hat{y}_n$, can be expressed as the multiplication of the corresponding incident signal, denoted by $\hat{x}_n$, and a complex reflection coefficient,[2] i.e.,

$$\hat{y}_n = \beta_n e^{j\theta_n}\hat{x}_n, \quad n \in \mathcal{N}, \tag{1}$$

where $\beta_n \in [0,1]$ and $\theta_n \in [-2\pi, 0)$ are the reflection amplitude and phase shift of element n, respectively. Note that θ_n's are periodic with respect to 2π, thus we consider them in $[0, 2\pi)$ for convenience in the sequel of this paper. As such, the IRS with N elements performs a linear mapping from the incident signal vector to a reflected signal vector based on an equivalent $N \times N$ diagonal phase-shift matrix $\boldsymbol{\Theta}$, i.e., $\hat{\boldsymbol{y}} = \boldsymbol{\Theta}\hat{\boldsymbol{x}}$, where $\boldsymbol{\Theta} = \text{diag}(\beta_1\ e^{j\theta_1}, \cdots, \beta_N e^{j\theta_N})$, $\hat{\boldsymbol{x}} = [\hat{x}_1, \cdots, \hat{x}_N]^T$, and $\hat{\boldsymbol{y}} = [\hat{y}_1, \cdots, \hat{y}_N]^T$. Theoretically, the reflection amplitude of each element can be adjusted for different purposes such as channel estimation, energy harvesting, and performance optimization [6]. However, in practice, it is costly to implement independent control of the reflection amplitude and phase shift simultaneously; thus, each element is usually designed to maximize the signal reflection for simplicity [6], [7], [29], [30], [32]. As such, we assume $\beta_n = 1, \forall n \in \mathcal{N}$, in the sequel of this paper. For ease of practical implementation, we also consider that the phase shift at each element of the IRS can take only a finite number of discrete values. Let b denote the number of bits used to indicate the number of phase shift levels L where $L = 2^b$. For simplicity, we assume that such discrete phase-shift values are obtained by uniformly quantizing the interval $[0, 2\pi)$. Thus, the set of discrete phase-shift values at each element is given by

$$\mathcal{F} = \{0, \Delta\theta, \cdots, (L-1)\Delta\theta\}, \tag{2}$$

where $\Delta\theta = 2\pi/L$. Note that for an IRS with N elements each with L phase shift levels, a total number of L^N beam patterns can be realized.

Denote by $\boldsymbol{h}_{d,k}^H \in \mathbb{C}^{1\times M}$, $\boldsymbol{h}_{r,k}^H \in \mathbb{C}^{1\times N}$, and $\boldsymbol{G} \in \mathbb{C}^{N\times M}$ the baseband equivalent channels from the AP to user k, the IRS to user k, and the AP to IRS, respectively. At the AP, we consider the conventional continuous linear precoding with $\boldsymbol{w}_k \in \mathbb{C}^{M\times 1}$ denoting the transmit precoding vector for user k. The complex baseband transmitted signal at the AP can be then expressed as $\boldsymbol{x} = \sum_{k=1}^K \boldsymbol{w}_k s_k$ where s_k's denote the information-bearing symbols of users which are modelled as independent and identically distributed (i.i.d.) random variables with zero mean and unit variance. Accordingly, the total transmit power consumed at the AP is given by

$$P = \sum_{k=1}^K \|\boldsymbol{w}_k\|^2. \tag{3}$$

For user k, the signal directly coming from the AP and that reflected by the IRS are combined at the receiver and thus the received signal can be expressed as

$$y_k = (\boldsymbol{h}_{r,k}^H \boldsymbol{\Theta}\boldsymbol{G} + \boldsymbol{h}_{d,k}^H)\sum_{j=1}^K \boldsymbol{w}_j s_j + z_k, \quad k \in \mathcal{K}, \tag{4}$$

where z_k denotes i.i.d. additive white Gaussian noise (AWGN) at user k's receiver with zero mean and variance σ_k^2. The SINR of user k is thus given by

$$\text{SINR}_k = \frac{|(\boldsymbol{h}_{r,k}^H \boldsymbol{\Theta}\boldsymbol{G} + \boldsymbol{h}_{d,k}^H)\boldsymbol{w}_k|^2}{\sum_{j\neq k}^K |(\boldsymbol{h}_{r,k}^H \boldsymbol{\Theta}\boldsymbol{G} + \boldsymbol{h}_{d,k}^H)\boldsymbol{w}_j|^2 + \sigma_k^2}, \quad k \in \mathcal{K}. \tag{5}$$

Remark 1: Note that (5) provides a general expression of the SINR for a user at arbitrary location in the IRS-aided single-cell system considered in this paper. While in practice, if user m, $m \in \mathcal{K}$, is sufficiently far from the passive IRS, the reflection of the IRS can be ignored and its SINR is approximated by $\text{SINR}_m \approx \frac{|\boldsymbol{h}_{d,m}^H \boldsymbol{w}_m|^2}{\sum_{j\neq m}^K |\boldsymbol{h}_{d,m}^H \boldsymbol{w}_j|^2 + \sigma_m^2}$, which corresponds to the traditional case where user m is served by the AP via transmit precoding only without the IRS. Although the phase-shift matrix $\boldsymbol{\Theta}$ does not directly affect the SINR of user m in this case, it can have an indirect effect on it via balancing the SINRs of those users nearby the IRS as shown in (5) and thereby adjusting their AP transmit precoding vectors, which then contribute to the interference at user m's receiver.

B. Problem Formulation

Denote by $\gamma_k > 0$ the minimum SINR requirement of user $k, k \in \mathcal{K}$. Let $\boldsymbol{\theta} = [\theta_1, \cdots, \theta_N]$ and $\boldsymbol{W} = [\boldsymbol{w}_1, \cdots, \boldsymbol{w}_K] \in \mathbb{C}^{M\times K}$. In this paper, we aim to minimize the total transmit power at the AP by jointly optimizing the transmit precoders $\boldsymbol{W}$ at the AP and phase shifts $\boldsymbol{\theta}$ at the IRS, subject to the user SINR constraints as well as the IRS discrete phase-shift constraints. The corresponding optimization problem is formulated as

$$(\text{P1}): \min_{\boldsymbol{W},\boldsymbol{\theta}} \sum_{k=1}^K \|\boldsymbol{w}_k\|^2 \tag{6}$$

$$\text{s.t.} \ \frac{|(\boldsymbol{h}_{r,k}^H \boldsymbol{\Theta}\boldsymbol{G} + \boldsymbol{h}_{d,k}^H)\boldsymbol{w}_k|^2}{\sum_{j\neq k}^K |(\boldsymbol{h}_{r,k}^H \boldsymbol{\Theta}\boldsymbol{G} + \boldsymbol{h}_{d,k}^H)\boldsymbol{w}_j|^2 + \sigma_k^2} \geq \gamma_k, \quad \forall k \in \mathcal{K}, \tag{7}$$

$$\theta_n \in \mathcal{F} = \{0, \Delta\theta, \cdots, (L-1)\Delta\theta\}, \quad \forall n \in \mathcal{N}. \tag{8}$$

Note that the constraints in (7) are non-convex due to the coupling of $\boldsymbol{W}$ and $\boldsymbol{\theta}$ in users' SINR expressions. In addition, the constraints in (8) restrict θ_n's to be discrete values. As a result, problem (P1) is an MINLP which is generally NP-hard, and

[1] In general, there are two main approaches for the IRS-involved channel acquisition, depending on whether the IRS elements are equipped with receive RF chains or not [6]. For the first approach with receive RF chains, conventional channel estimation methods can be applied for the IRS to estimate the channels of the AP-IRS and IRS-user links, respectively. In contrast, for the second approach without receive RF chains at the IRS, the IRS reflection patterns can be designed together with the uplink pilots to estimate the concatenated AP-IRS-user channels [18], [36]. The proposed beamforming designs in this paper are applicable with both the above channel estimation methods.

[2] For convenience, we use the equivalent baseband signal model to represent the actual signal reflection at IRS in the RF band.

there is no standard method for obtaining its globally optimal solution efficiently [37], [38]. One commonly used approach is to first solve problem (P1) with all discrete optimization variables θ_n's relaxed to their continuous counterparts and then directly quantize each of the obtained continuous phase shifts to its nearest discrete value in $\mathcal{F}$ [1]. However, even after such relaxation, (P1) is still a non-convex optimization problem [7]. Furthermore, such a direct quantization method may be ineffective for the practical IRS with low-resolution phase shifters (e.g., $b = 1$), especially in the multiuser case with severe co-channel interference (as will be shown later in Section V). Nevertheless, this suboptimal quantization approach will be used in Section III-C to characterize the performance of the IRS with discrete phase shifts in the regime of asymptotically large N as compared to the ideal case with continuous phase shifts.

III. Single-User System

First, we consider the single-user setup, i.e., $K = 1$, where there is only one user in the considered time-frequency dimension. This corresponds to the practical scenario when orthogonal multiple access (such as time division multiple access) is employed to separate the communications for different users. Due to the absence of multiuser interference, (P1) is simplified to (by dropping the user index)

$$\min_{\boldsymbol{w},\boldsymbol{\theta}} \ \|\boldsymbol{w}\|^2 \tag{9}$$

$$\text{s.t. } |(\boldsymbol{h}_r^H\boldsymbol{\Theta}\boldsymbol{G}+\boldsymbol{h}_d^H)\boldsymbol{w}|^2 \geq \gamma\sigma^2, \tag{10}$$

$$\theta_n \in \mathcal{F}, \forall n \in \mathcal{N}. \tag{11}$$

For any given phase shifts $\boldsymbol{\theta}$, it is known that the maximum-ratio transmission (MRT) is the optimal transmit precoder to problem (9) [39], i.e., $\boldsymbol{w}^* = \sqrt{P}\frac{(\boldsymbol{h}_r^H\boldsymbol{\Theta}\boldsymbol{G}+\boldsymbol{h}_d^H)^H}{\|\boldsymbol{h}_r^H\boldsymbol{\Theta}\boldsymbol{G}+\boldsymbol{h}_d^H\|}$. By substituting $\boldsymbol{w}^*$ into problem (9), we obtain the optimal transmit power as $P^* = \frac{\gamma\sigma^2}{\|\boldsymbol{h}_r^H\boldsymbol{\Theta}\boldsymbol{G}+\boldsymbol{h}_d^H\|^2}$. As such, minimizing the AP transmit power is equivalent to maximizing the channel power gain of the combined user channel, i.e.,

$$\max_{\boldsymbol{\theta}} \ \|\boldsymbol{h}_r^H\boldsymbol{\Theta}\boldsymbol{G}+\boldsymbol{h}_d^H\|^2 \tag{12}$$

$$\text{s.t. } \theta_n \in \mathcal{F}, \forall n \in \mathcal{N}. \tag{13}$$

By applying the change of variables $\boldsymbol{h}_r^H\boldsymbol{\Theta}\boldsymbol{G} = \boldsymbol{v}^H\boldsymbol{\Phi}$ where $\boldsymbol{v} = [e^{j\theta_1}, \cdots, e^{j\theta_N}]^H$ and $\boldsymbol{\Phi} = \text{diag}(\boldsymbol{h}_r^H)\boldsymbol{G} \in \mathbb{C}^{N\times M}$, we have $\|\boldsymbol{h}_r^H\boldsymbol{\Theta}\boldsymbol{G}+\boldsymbol{h}_d^H\|^2 = \|\boldsymbol{v}^H\boldsymbol{\Phi}+\boldsymbol{h}_d^H\|^2$. Let $\boldsymbol{A} = \boldsymbol{\Phi}\boldsymbol{\Phi}^H$ and $\hat{\boldsymbol{h}}_d = \boldsymbol{\Phi}\boldsymbol{h}_d$. Problem (12) is thus equivalent to

$$\text{(P2)}: \ \max_{\boldsymbol{\theta}} \ \boldsymbol{v}^H\boldsymbol{A}\boldsymbol{v} + 2\text{Re}\{\boldsymbol{v}^H\hat{\boldsymbol{h}}_d\} + \|\boldsymbol{h}_d^H\|^2 \tag{14}$$

$$\text{s.t. } \theta_n \in \mathcal{F}, \forall n \in \mathcal{N}. \tag{15}$$

Although (P2) is still non-convex, we obtain its optimal and high-quality suboptimal solutions by exploiting its special structure.

A. Optimal Solution

We first show that problem (P2) can be reformulated as an ILP for which the globally optimal solution can be obtained by applying the branch-and-bound method. Specifically, we exploit the special ordered set of type 1 (SOS1) [38] and transform (P2) into a linear program with only binary optimization variables. The formal definition of SOS1 is given as follows.

Definition 1: A special ordered set of type 1 (SOS1) is a set of vectors with length N, each of which has only one entry being 1 with the others being 0 [38], i.e.,

$$\sum_{i=1}^{N} \boldsymbol{x}(i) = 1, \boldsymbol{x}(i) \in \{0,1\}. \tag{16}$$

The SOS1 vector is useful in expressing an optimization variable that belongs to a set with discrete variables. By applying some algebra operations using the fact that $\boldsymbol{A}$ is positive semi-definite, the objective function of (P2) can be expanded as (by ignoring the constant terms)

$$\begin{aligned}
&\mathcal{G}(\boldsymbol{\theta}, \phi_{i,n}) \\
&\triangleq \sum_{i=1}^{N-1}\sum_{n=i+1}^{N} 2|\boldsymbol{A}(i,n)|\big(\cos(\arg(\boldsymbol{A}(i,n)))\cos(\phi_{i,n}) \\
&\quad - \sin(\arg(\boldsymbol{A}(i,n)))\sin(\phi_{i,n})\big) \\
&\quad + 2\sum_{n=1}^{N} |\hat{\boldsymbol{h}}_d(n)|\big(\cos(\arg(\hat{\boldsymbol{h}}_d(n)))\cos(\theta_n) \\
&\quad - \sin(\arg(\hat{\boldsymbol{h}}_d(n)))\sin(\theta_n)\big) + \sum_{n=1}^{N}\boldsymbol{A}(n,n),
\end{aligned} \tag{17}$$

where $\phi_{i,n} = \theta_i - \theta_n, i, n \in \mathcal{N}$. As such, problem (P2) is equivalent to

$$\max_{\boldsymbol{\theta},\{\phi_{i,n}\}} \ \mathcal{G}(\boldsymbol{\theta}, \phi_{i,n}) \tag{18}$$

$$\text{s.t. } \theta_n \in \mathcal{F}, \forall n \in \mathcal{N}, \tag{19}$$

$$\phi_{i,n} = \theta_i - \theta_n, \quad \forall i, \ n \in \mathcal{N}. \tag{20}$$

Let $\mathbf{a} = [0, \Delta\theta, \cdots, (L-1)\Delta\theta]^T$, $\mathbf{c} = [1, \cos(\Delta\theta), \cdots, \cos((L-1)\Delta\theta)]^T$, and $\mathbf{s} = [1, \sin(\Delta\theta), \cdots, \sin((L-1)\Delta\theta)]^T$. Note that $\cos(\phi_{i,n})$, $\sin(\phi_{i,n})$, $\cos(\theta_n)$, and $\sin(\theta_n)$ in $\mathcal{G}(\boldsymbol{\theta}, \phi_{i,n})$ are all non-linear functions with respect to the associated optimization variables. To overcome this issue, we introduce an SOS1 binary vector $\boldsymbol{x}_n$ for element n of the IRS. Accordingly, θ_n, $\cos(\theta_n)$, and $\sin(\theta_n)$ can be expressed in the linear form of $\boldsymbol{x}_n$, i.e.,

$$\theta_n = \mathbf{a}^T\boldsymbol{x}_n, \quad \cos(\theta_n) = \mathbf{c}^T\boldsymbol{x}_n, \ \ \sin(\theta_n) = \mathbf{s}^T\boldsymbol{x}_n. \tag{21}$$

Similarly, for the phase-shift difference of two elements i and n, i.e., $\phi_{i,n}$, we introduce an SOS1 binary vector $\boldsymbol{y}_{i,n}$. Since the value of θ_n is chosen from $\mathcal{F}$, all the possible values of $\phi_{i,n} = \theta_i - \theta_n \in (-2\pi, 2\pi)$ belongs to the set $\hat{\mathcal{F}} = \{-(L-1)\Delta\theta, \cdots, -\Delta\theta, 0, \Delta\theta, \cdots, (L-1)\Delta\theta\}$. To overcome the phase ambiguity of $\phi_{i,n}$ with respect to 2π, we further introduce a binary variable $\varepsilon_{i,n}$ which takes the value of 0 when $\theta_i - \theta_n$ belongs to $[0, 2\pi)$ and 1 otherwise. As such, all the possible values of $\phi_{i,n}$ are restricted to the set $\mathcal{F}$ and accordingly we have

$$\phi_{i,n} = \mathbf{a}^T\boldsymbol{y}_{i,n} - 2\pi\varepsilon_{i,n}, \cos(\phi_{i,n}) = \mathbf{c}^T\boldsymbol{y}_{i,n}, \sin(\phi_{i,n}) = \mathbf{s}^T\boldsymbol{y}_{i,n}. \tag{22}$$

Substituting (21) and (22) into problem (18), we obtain the following optimization problem

$$\max_{\{\boldsymbol{x}_n\},\{\boldsymbol{y}_{i,n}\},\{\varepsilon_{i,n}\}} \sum_{i=1}^{N-1}\sum_{n=i+1}^{N} 2|\boldsymbol{A}(i,n)|\big(\cos(\arg(\boldsymbol{A}(i,n)))\mathbf{c}^T - \sin(\arg(\boldsymbol{A}(i,n)))\mathbf{s}^T\big)\boldsymbol{y}_{i,n} + 2\sum_{n=1}^{N}|\hat{\boldsymbol{h}}_d(n)|(\cos(\arg(\hat{\boldsymbol{h}}_d(n)))\mathbf{c}^T - \sin(\arg(\hat{\boldsymbol{h}}_d(n)))\mathbf{s}^T)\boldsymbol{x}_n \quad (23)$$

$$\text{s.t. } \mathbf{a}^T(\boldsymbol{x}_i-\boldsymbol{x}_n)+2\pi\varepsilon_{i,n}=\mathbf{a}^T\boldsymbol{y}_{i,n}, \quad \forall i,\ n\in\mathcal{N}, \quad (24)$$

$$\boldsymbol{x}_n \in SOS1, \quad \boldsymbol{y}_{i,n}\in SOS1,$$
$$\varepsilon_{i,n}\in\{0,1\}, \quad \forall i,\ n\in\mathcal{N}. \quad (25)$$

It is not difficult to show that problem (23) is an ILP and thus can be optimally solved by applying the branch-and-bound method [38].

B. Suboptimal Solution

Although the optimal solution to (P2) can be obtained as in the previous subsection, the worst-case complexity is still exponential over N due to its fundamental NP-hardness. To reduce the computational complexity, we propose in this subsection an efficient successive refinement algorithm to solve (P2) sub-optimally, which will also be extended to the general multiuser case in Section IV. Specifically, we alternately optimize each of the N phase shifts in an iterative manner by fixing the other $N-1$ phase shifts, until the convergence is achieved.

The key to solving (P2) by applying the successive refinement algorithm lies in the observation that for a given $n\in\mathcal{N}$, by fixing θ_ℓ's, $\forall \ell\neq n, \ell\in\mathcal{N}$, the objective function of (P2) is linear with respect to $e^{j\theta_n}$, which can be written as

$$2\mathrm{Re}\left\{e^{j\theta_n}\zeta_n\right\}+\sum_{\ell\neq n}^{N}\sum_{i\neq n}^{N}\boldsymbol{A}(\ell,i)e^{j(\theta_\ell-\theta_i)}+C, \quad (26)$$

where ζ_n and C are constants given by

$$\zeta_n=\sum_{\ell\neq n}^{N}\boldsymbol{A}(n,\ell)e^{-j\theta_\ell}+\hat{\boldsymbol{h}}_d(n)\triangleq|\zeta_n|e^{-j\varphi_n}, \quad (27)$$

$$C=\boldsymbol{A}(n,n)+2\mathrm{Re}\Big\{\sum_{\ell\neq n}^{N}e^{j\theta_\ell}\hat{\boldsymbol{h}}_d(\ell)\Big\}+\|\hat{\boldsymbol{h}}_d\|^2. \quad (28)$$

Based on (26) and (27), it is not difficult to verify that the optimal nth phase shift is given by

$$\theta_n^*=\arg\min_{\theta\in\mathcal{F}}|\theta-\varphi_n|. \quad (29)$$

By successively setting the phase shifts of all elements based on (29), the objective value of (P2) will be non-decreasing over the iterations. On the other hand, the optimal objective value of (P2) is upper-bounded by a finite value, i.e.,

$$\boldsymbol{v}^H\boldsymbol{A}\boldsymbol{v}+2\mathrm{Re}\{\boldsymbol{v}^H\hat{\boldsymbol{h}}_d\}+\|\boldsymbol{h}_d^H\|^2 \overset{(a)}{\leq} N\lambda_{\max}(\boldsymbol{A})+2\sum_{n=1}^{N}|\hat{\boldsymbol{h}}_d^H(n)|+\|\boldsymbol{h}_d^H\|^2, \quad (30)$$

where $\lambda_{\max}(\boldsymbol{A})$ is the maximum eigenvalue of $\boldsymbol{A}$ and the inequality (a) holds due to $\boldsymbol{v}^H\boldsymbol{A}\boldsymbol{v}\leq N\lambda_{\max}(\boldsymbol{A})$ and $\mathrm{Re}\{\boldsymbol{v}^H\hat{\boldsymbol{h}}_d\}\leq\sum_{n=1}^{N}|\hat{\boldsymbol{h}}_d^H(n)|$. Therefore, the proposed algorithm is guaranteed to converge. With the converged discrete phase shifts, the minimum transmit power P^* can be obtained accordingly.

C. Performance Analysis for IRS With Asymptotically Large N

Next, we characterize the scaling law of the average received power at the user with respect to the number of reflecting elements, N, as $N\to\infty$ in an IRS-aided system with discrete phase shifts. For simplicity, we assume $M=1$ with $\boldsymbol{G}\equiv\boldsymbol{g}$ to obtain essential insight. Besides, the signal received at the user from the AP-user link can be practically ignored for asymptotically large N since in this case, the reflected signal power dominates in the total received power. Thus, the user's average received power with b-bit phase shifters is approximately given by $P_r(b)\triangleq P\mathbb{E}(|h^H|^2)=P\mathbb{E}(|\boldsymbol{h}_r^H\boldsymbol{\Theta}\boldsymbol{g}|^2)$ where $\boldsymbol{\theta}$ is assumed to be obtained by quantizing each of the optimal continuous phase shifts obtained in [13] to its nearest discrete value in $\mathcal{F}$.

Proposition 1: Assume $\boldsymbol{h}_r^H\sim\mathcal{CN}(\mathbf{0},\varrho_h^2\boldsymbol{I})$ and $\boldsymbol{g}\sim\mathcal{CN}(\mathbf{0},\varrho_g^2\boldsymbol{I})$. As $N\to\infty$, we have[3]

$$\eta(b)\triangleq\frac{P_r(b)}{P_r(\infty)}=\Big(\frac{2^b}{\pi}\sin\Big(\frac{\pi}{2^b}\Big)\Big)^2. \quad (31)$$

Proof: The combined user channel can be expressed as

$$h^H=\boldsymbol{h}_r^H\boldsymbol{\Theta}\boldsymbol{g}=\sum_{n=1}^{N}|\boldsymbol{h}_r^H(n)||\boldsymbol{g}(n)|e^{j(\theta_n+\phi_n+\psi_n)}, \quad (32)$$

where $\boldsymbol{h}_r^H(n)=|\boldsymbol{h}_r^H(n)|e^{j\phi_n}$ and $\boldsymbol{g}(n)=|\boldsymbol{g}(n)|e^{j\psi_n}$, respectively. Since $|\boldsymbol{h}_r^H(n)|$ and $|\boldsymbol{g}(n)|$ are statistically independent and follow Rayleigh distribution with mean values $\sqrt{\pi}\varrho_h/2$ and $\sqrt{\pi}\varrho_g/2$, respectively, we have $\mathbb{E}(|\boldsymbol{h}_r^H(n)||\boldsymbol{g}(n)|)=\pi\varrho_h\varrho_g/4$. Since ϕ_n and ψ_n are randomly and uniformly distributed in $[0,2\pi)$, it follows that $\phi_n+\psi_n$ is uniformly distributed in $[0,2\pi)$ due to the periodicity over 2π. As such, the optimal continuous phase shift is given by $\theta_n^\star=-(\phi_n+\psi_n)$, $n\in\mathcal{N}$ [13], with the corresponding quantized discrete phase shift denoted by $\hat{\theta}_n$ which can be obtained similarly as (29). Define $\bar{\theta}_n=\hat{\theta}_n-\theta_n^\star=\hat{\theta}_n+\phi_n+\psi_n$ as the quantization error. As $\hat{\theta}_n$'s in $\mathcal{F}$ are equally spaced, it follows that $\bar{\theta}_n$'s are independently and uniformly distributed in $[-\pi/2^b,\pi/2^b)$.

[3]It is worth pointing out that $N\to\infty$ is not physically achievable due to energy conservation whereas the purpose of the asymptotic analysis here is to reveal the power scaling behavior, similarly to that for massive MIMO [19], [40]. It will be shown later in Section V that this result is valid for moderately large N in practice.

TABLE I
THE POWER LOSS OF USING IRS WITH DISCRETE PHASE SHIFTS

Number of control bits: b	$b=1$	$b=2$	$b=3$	$b=\infty$ (continuous phase shifts)
Power loss: $1/\left(\frac{2^b}{\pi}\sin\left(\frac{\pi}{2^b}\right)\right)^2$	3.9 dB	0.9 dB	0.2 dB	0 dB

Thus, we have

$$\begin{aligned}\mathbb{E}(|h^H|^2) &= \mathbb{E}\left(\left|\sum_{n=1}^{N}|\boldsymbol{h}_r^H(n)||\boldsymbol{g}(n)|e^{j\bar{\theta}_n}\right|^2\right)\\ &= \mathbb{E}\left(\sum_{n=1}^{N}\sum_{i\neq n}^{N}|\boldsymbol{h}_r^H(n)||\boldsymbol{g}(n)||\boldsymbol{h}_r^H(i)||\boldsymbol{g}(i)|e^{j\bar{\theta}_n-j\bar{\theta}_i}\right.\\ &\quad\left.+\sum_{n=1}^{N}|\boldsymbol{h}_r^H(n)|^2|\boldsymbol{g}(n)|^2\right). \end{aligned} \tag{33}$$

Note that $\boldsymbol{h}_r^H(n)$, $\boldsymbol{g}(n)$, and $e^{j\bar{\theta}_n}$ are independent with each other, with $\mathbb{E}\left(\sum_{n=1}^{N}|\boldsymbol{h}_r^H(n)|^2|\boldsymbol{g}(n)|^2\right) = N\varrho_h^2\varrho_g^2$ and $\mathbb{E}(e^{j\bar{\theta}_n}) = \mathbb{E}(e^{-j\bar{\theta}_n}) = 2^b/\pi\sin\left(\pi/2^b\right)$. It then follows that

$$P_r(b) = NP\varrho_h^2\varrho_g^2 + N(N-1)P\frac{\pi^2\varrho_h^2\varrho_g^2}{16}\left(\frac{2^b}{\pi}\sin\left(\frac{\pi}{2^b}\right)\right)^2. \tag{34}$$

For $b \geq 1$, it is not difficult to verify that $2^b/\pi\sin\left(\pi/2^b\right)$ increases with b monotonically and satisfies

$$\lim_{b\to\infty}\frac{2^b}{\pi}\sin\left(\frac{\pi}{2^b}\right) = 1, \tag{35}$$

where $b\to\infty$ corresponds to the case of continuous phase shifts without quantization. As a result, the ratio between $P_r(b)$ and $P_r(\infty)$ is given by (31) as $N\to\infty$, which completes the proof. ■

Proposition 1 provides a quantitative measure of the user received power loss with discrete phase shifts as compared to the ideal case with continuous phase shifts. It is observed that as $N\to\infty$, the power ratio $\eta(b)$ depends only on the number of discrete phase-shift levels, 2^b, but is regardless of N. This result implies that using a practical IRS even with discrete phase shifts, the same asymptotic *squared power gain* of $\mathcal{O}(N^2)$ as that with continuous phase shifts shown in [13] can still be achieved (see (34) with $N\to\infty$). As such, the design of IRS hardware and control module can be greatly simplified by using discrete phase shifters, without compromising the performance in the large-N regime. Since $\eta(1) = -3.9$ dB, $\eta(2) = -0.9$ dB, and $\eta(3) = -0.2$ dB as shown in Table I, using 2 or 3-bit phase shifters is practically sufficient to achieve close-to-optimal performance with only approximately 0.9 dB or 0.2 dB power loss. In general, there exists an interesting cost tradeoff between the number of reflecting elements (N) and the resolution of phase shifters (2^b) used at the IRS. For example, one can use more reflecting elements (larger N) each with a lower-resolution (smaller b) phase shifter (thus lower cost per element), or less number of elements (smaller N) with higher-resolution (larger b) phase-shifters (i.e., higher cost per element), to achieve the same received power at the user. As such, N and b can be flexibly set in practical systems based on the required performance as well as the manufacturing cost of each reflecting element and that of its phase shifter component so as to minimize the total cost of the IRS.

Remark 2: Consider a typical path loss model with $\varrho_h^2 = C_0 d_{Iu}^{-\alpha}$ where C_0 is the path loss at the reference distance of 1 meter (m), d_{Iu} is the IRS-user link distance, and α denotes the path loss exponent. Based on (34), it is interesting to note that when N is sufficiently large, we have

$$P_r \approx N^2\frac{P\pi^2\varrho_h^2\varrho_g^2}{16}\left(\frac{2^b}{\pi}\sin\left(\frac{\pi}{2^b}\right)\right)^2. \tag{36}$$

By substituting ϱ_h^2 into (36), it follows that

$$N \approx d_{Iu}^{\frac{\alpha}{2}}C_1, \tag{37}$$

where $C_1 = \sqrt{\frac{P_r}{PC_0}}\frac{4}{\varrho_g 2^b\sin\left(\frac{\pi}{2^b}\right)}$. From (37), it can be observed that as the user moves away from the IRS, i.e., d_{Iu} increases, the number of elements at the IRS needs to be increased to keep the same user receive power without increasing the transmit power, e.g., by increasing N linearly with d_{Iu} if $\alpha = 2$.

IV. MULTIUSER SYSTEM

In this section, we study the general multiuser setup where multiple users share the same time-frequency dimension for communications (e.g., in space division multiple access) and they are located at arbitrary locations in the single-cell network among which only some are aided by the nearby IRS in general. For this general setup, we propose two algorithms to obtain the optimal and suboptimal solutions to (P1), respectively.

A. Optimal Solution

For any given phase shifts $\boldsymbol{\theta}$, the combined channel from the AP to user k is denoted by $\boldsymbol{h}_k^H \triangleq \boldsymbol{h}_{r,k}^H\boldsymbol{\Theta}\boldsymbol{G} + \boldsymbol{h}_{d,k}^H$. Thus, problem (P1) is reduced to

$$(\text{P3}): \quad \min_{\boldsymbol{W}} \sum_{k=1}^{K}\|\boldsymbol{w}_k\|^2 \tag{38}$$

$$\text{s.t. } \frac{|\boldsymbol{h}_k^H\boldsymbol{w}_k|^2}{\sum_{j\neq k}^{K}|\boldsymbol{h}_k^H\boldsymbol{w}_j|^2 + \sigma_k^2} \geq \gamma_k, \quad \forall k\in\mathcal{K}. \tag{39}$$

Note that (P3) is the conventional power minimization problem in the multiuser MISO downlink broadcast channel, which can be efficiently and optimally solved by using the fixed-point iteration algorithm based on the uplink-downlink duality [41]–[43]. Specifically, the optimal solution is known as the

minimum mean squared error (MMSE) based linear precoder given by

$$\boldsymbol{w}_k^* = \sqrt{p_k}\hat{\boldsymbol{w}}_k^*, \quad \forall k \in \mathcal{K}. \tag{40}$$

where

$$\begin{bmatrix} p_1 \\ \vdots \\ p_K \end{bmatrix} = \boldsymbol{Q}^{-1} \begin{bmatrix} \sigma_1^2 \\ \vdots \\ \sigma_K^2 \end{bmatrix}, \tag{41}$$

$$\boldsymbol{Q}(i,j) = \begin{cases} \frac{1}{\gamma_i}|\boldsymbol{h}_i^H \hat{\boldsymbol{w}}_i^*|^2, & i = j, \\ -|\boldsymbol{h}_i^H \hat{\boldsymbol{w}}_j^*|^2, & i \neq j, \forall i, j \in \mathcal{K}, \end{cases} \tag{42}$$

$$\hat{\boldsymbol{w}}_k^* = \frac{(\boldsymbol{I}_M + \sum_{i=1}^K \frac{\lambda_i}{\sigma_i^2}\boldsymbol{h}_i\boldsymbol{h}_i^H)^{-1}\boldsymbol{h}_k}{||(\boldsymbol{I}_M + \sum_{i=1}^K \frac{\lambda_i}{\sigma_i^2}\boldsymbol{h}_i\boldsymbol{h}_i^H)^{-1}\boldsymbol{h}_k||}, \forall k, \tag{43}$$

$$\lambda_k = \frac{\sigma_k^2}{(1+\frac{1}{\gamma_k})\boldsymbol{h}_k^H(\boldsymbol{I}_M + \sum_{i=1}^K \frac{\lambda_i}{\sigma_i^2}\boldsymbol{h}_i\boldsymbol{h}_i^H)^{-1}\boldsymbol{h}_k}, \forall k. \tag{44}$$

First, all λ_k's can be obtained by using the fixed-point algorithm to solve K equations in (44). With λ_k's, $\hat{\boldsymbol{w}}_k^*$'s can be obtained from (43) and then p_k's can be obtained from (41). Finally, $\boldsymbol{w}_k^*$'s are obtained by using (40) with $\hat{\boldsymbol{w}}_k^*$'s and p_k's.

As shown in (40)-(44), the optimal transmit precoder $\boldsymbol{W}$ cannot be expressed as a closed-form expression of $\boldsymbol{\theta}$ as in the single-user case (i.e., the MRT precoder in Section III) and thus transforming (P1) into an ILP is impossible to our best knowledge. As such, the globally optimal phase shifts to (P1) can only be obtained by the exhaustive search method. Specifically, we can search all the possible cases of $\boldsymbol{\theta}$ and for each case, we solve (P3) to obtain the corresponding transmit power at the AP. The globally optimal $\boldsymbol{\theta}$ is then given by the one that achieves the minimum AP transmit power. As the optimal algorithm requires computing the MMSE precoder $\boldsymbol{W}$ and exhaustively searching the phase shifts $\boldsymbol{\theta}$, the total complexity for it can be shown to be $\mathcal{O}(L^N(I_{itr}(KM^2 + M^3) + K^3 + K^2M + KMN))$ where I_{itr} denotes the number of iterations required for obtaining λ_k's in (44) in each case (which is observed to increase with K linearly in our simulations).

B. Suboptimal Solution

To reduce the computational complexity of the optimal solution, we extend the successive refinement algorithm in Section III-B to the multiuser case, assuming $M \geq K$.[4] Specifically, the suboptimal ZF-based linear precoder is employed at the AP to eliminate the multiuser interference and meet all the SINR requirements. Then the phase shifts at the IRS are successively refined to minimize the total transmit power at the AP.

With the combined channel $\boldsymbol{h}_k^H$'s, $k \in \mathcal{K}$, the corresponding ZF constraints are given by $\boldsymbol{h}_k^H\boldsymbol{w}_j = (\boldsymbol{h}_{r,k}^H\boldsymbol{\Theta}\boldsymbol{G} + \boldsymbol{h}_{d,k}^H)\boldsymbol{w}_j = 0$, $\forall j \neq k, j \in \mathcal{K}$. Let $\boldsymbol{H}^H = \boldsymbol{H}_r^H\boldsymbol{\Theta}\boldsymbol{G} + \boldsymbol{H}_d^H$, where $\boldsymbol{H}_r^H = [\boldsymbol{h}_{r,1}, \cdots, \boldsymbol{h}_{r,K}]^H$ and $\boldsymbol{H}_d^H = [\boldsymbol{h}_{d,1}, \cdots, \boldsymbol{h}_{d,K}]^H$. With those additional constraints, it is not difficult to verify that the optimal transmit precoder $\boldsymbol{W}$ to (P1) is given by the pseudo-inverse of the combined channel $\boldsymbol{H}^H$ with proper power allocation among different users, i.e.,

$$\boldsymbol{W} = \boldsymbol{H}(\boldsymbol{H}^H\boldsymbol{H})^{-1}\boldsymbol{P}^{\frac{1}{2}}, \tag{45}$$

where $\boldsymbol{P} = \mathrm{diag}(p_1, \cdots, p_K)$ is the power allocation matrix. By substituting $\boldsymbol{W}$ into (7) in (P1), the SINR constraint of user k is reduced to $\frac{p_k}{\sigma_k^2} \geq \gamma_k, \forall k \in \mathcal{K}$. Since this constraint should be met with equality at the optimal solution to (P1), we have $p_k = \sigma_k^2\gamma_k, k \in \mathcal{K}$. The total transmit power at the AP is then given by

$$\sum_{k=1}^K \|\boldsymbol{w}_k\|^2 = \mathrm{tr}(\boldsymbol{P}^{\frac{1}{2}}(\boldsymbol{H}^H\boldsymbol{H})^{-1}\boldsymbol{P}^{\frac{1}{2}}) \overset{(a)}{=} \mathrm{tr}(\boldsymbol{P}(\boldsymbol{H}^H\boldsymbol{H})^{-1})$$
$$= \mathrm{tr}(\boldsymbol{P}((\boldsymbol{H}_r^H\boldsymbol{\Theta}\boldsymbol{G} + \boldsymbol{H}_d^H)(\boldsymbol{H}_r^H\boldsymbol{\Theta}\boldsymbol{G} + \boldsymbol{H}_d^H)^H)^{-1}), \tag{46}$$

where (a) is due to the fact that $\mathrm{tr}(\boldsymbol{A}\boldsymbol{B}) = \mathrm{tr}(\boldsymbol{B}\boldsymbol{A})$ for any matrices $\boldsymbol{A}$ and $\boldsymbol{B}$ with appropriate dimensions. As a result, (P1) is transformed to

$$\text{(P5)}: \min_{\boldsymbol{\theta}} \ \mathrm{tr}\Big(\boldsymbol{P}((\boldsymbol{H}_r^H\boldsymbol{\Theta}\boldsymbol{G} + \boldsymbol{H}_d^H) \times (\boldsymbol{H}_r^H\boldsymbol{\Theta}\boldsymbol{G} + \boldsymbol{H}_d^H)^H)^{-1}\Big) \triangleq P(\boldsymbol{\theta}) \tag{47}$$

$$\text{s.t. } \theta_n \in \mathcal{F}, \forall n \in \mathcal{N}. \tag{48}$$

Note that for $K = 1$, (P5) is equivalent to the combined channel power gain maximization problem, i.e., (P2), in the single-user case considered in Section III. However, in the multiuser case, (P5) becomes more involved than (P2) due to the matrix inverse operation that results in a more complicated non-convex objective function $P(\boldsymbol{\theta})$. Nevertheless, by fixing any $N-1$ phase shifts in each iteration, we can find the optimal solution of the remaining discrete phase shift via one-dimensional search over $\mathcal{F}$, i.e.,

$$\theta_n^* = \arg\min_{\theta_n \in \mathcal{F}} P(\boldsymbol{\theta}). \tag{49}$$

Note that for the above problem, if a rank-deficient channel matrix, i.e., $\mathrm{rank}(\boldsymbol{H}) < K$, is encountered for the optimization of some θ_n, then the corresponding value of $P(\boldsymbol{\theta})$ is set as positive infinity for tractability. Considering that the number of discrete phase-shift values in $\mathcal{F}$ is generally limited in practice [29], [30] (e.g., $L = 2$ for $b = 1$ or $L = 4$ for $b = 2$), the one-dimensional search in (49) is very efficient. The above procedure is repeated until the fractional decrease of $P(\boldsymbol{\theta})$ is less than a sufficiently small threshold. It can be similarly shown as in Section III-B that $P(\boldsymbol{\theta})$ is lower-bounded by a finite value and thus the convergence of the proposed ZF-based successive refinement algorithm is guaranteed.

In contrast to the optimal solution, the suboptimal solution is based on the ZF precoder at the AP and the successive refinement algorithm for finding the phase shifts at the IRS, thus its complexity is given by $\mathcal{O}(\hat{I}_{itr}L(K^3 + K^2M + KMN))$, where $\hat{I}_{itr}$ denotes the number of iterations required for achieving convergence of the successive refinement algorithm. Note that $K^3 + K^2M + KMN \leq I_{itr}(KM^2 + M^3) + K^3 + K^2M + KMN$ always holds, and $\hat{I}_{itr}L$ is usually much less than

[4]It is worth pointing out that if $M < K$, the MMSE precoding can be combined with the successive refinement algorithm to jointly optimize the transmit precoders and phase shifts, as will be shown later in Section V-B.

L^N in practice based on our simulations. Thus, the proposed suboptimal algorithm is computationally much more efficient for IRS with small L and large N, as compared to the optimal algorithm.

V. Numerical Results

In this section, we provide numerical results to validate our analysis as well as the effectiveness of the proposed algorithms. A three-dimensional (3D) coordinate is considered as shown in Fig. 2, where a uniform linear array (ULA) at the AP and a uniform rectangular array (URA) at the IRS are located in x-axis and y-z plane, respectively. The reference antenna/element at the AP/IRS are respectively located at $(d_x, 0, 0)$ and $(0, d_y, 0)$, where in both cases a half-wavelength spacing is assumed among adjacent antennas/elements. For the IRS, we set $N = N_y N_z$ where N_y and N_z denote the number of reflecting elements along y-axis and z-axis, respectively. For the purpose of exposition, we fix $N_y = 4$ and increase N_z linearly with N. The distance-dependent channel path loss is modeled as $C_0 d^{-\alpha}$ where d denotes the individual link distance. We adopt the spherical-wave model for all the channel links, which means that the link distance is calculated based on the 3D coordinate system described above. Each antenna at the AP is assumed to have an isotropic radiation pattern and thus the antenna gain is 0 dBi. In contrast, as the IRS reflects signals only in its front half-sphere, each reflecting element is assumed to have a 3 dBi gain for fair comparison. To account for small-scale fading, we assume the Rician fading channel model for all channels involved. For example, the AP-IRS channel $\boldsymbol{G}$ can be expressed as

$$\boldsymbol{G} = \sqrt{\frac{\beta_{\mathrm{AI}}}{1+\beta_{\mathrm{AI}}}}\boldsymbol{G}^{\mathrm{LoS}} + \sqrt{\frac{1}{1+\beta_{\mathrm{AI}}}}\boldsymbol{G}^{\mathrm{NLoS}}, \tag{50}$$

where β_{AI} is the Rician factor, and $\boldsymbol{G}^{\mathrm{LoS}}$ and $\boldsymbol{G}^{\mathrm{NLoS}}$ represent the deterministic LoS (specular) component and Rayleigh fading component with i.i.d. CSCG entries, respectively. Note that the above model is simplified to Rayleigh fading channel when $\beta_{\mathrm{AI}} = 0$ or LoS channel when $\beta_{\mathrm{AI}} \to \infty$. The entries in $\boldsymbol{G}$ are then multiplied by the square root of the distance-dependent path loss with the path loss exponent denoted by α_{AI}. The AP-user and IRS-user channels are similarly generated by following the above model. The path loss exponents of the AP-user and IRS-user links are denoted by α_{Au} and α_{Iu}, respectively, and the corresponding Rician factors are denoted by β_{Au} and β_{Iu}, respectively. In practice, the IRS is usually deployed to serve the users that suffer from severe signal attenuation in the AP-user channel and thus we set $\alpha_{\mathrm{Au}} = 3.5$ and $\beta_{\mathrm{Au}} = 0$, while their counterparts for AP-IRS and IRS-user channels will be properly specified later depending on the scenarios. Without loss of generality, we assume that all users have the same SINR target, i.e., $\gamma_k = \gamma, k \in \mathcal{K}$. The stopping threshold for the successive refinement algorithms is set as 10^{-4}. We consider a system that operates on a carrier frequency of 750 MHz with the system bandwidth of 1 MHz and the effective noise power density of -150 dBm/Hz for all users. Thus we have $C_0 = -30$ dB and $\sigma_k^2 = -90$ dBm, $k \in \mathcal{K}$. Other system parameters are set as follows unless specified later: $d_x = 2$ m and $d_y = 50$ m.

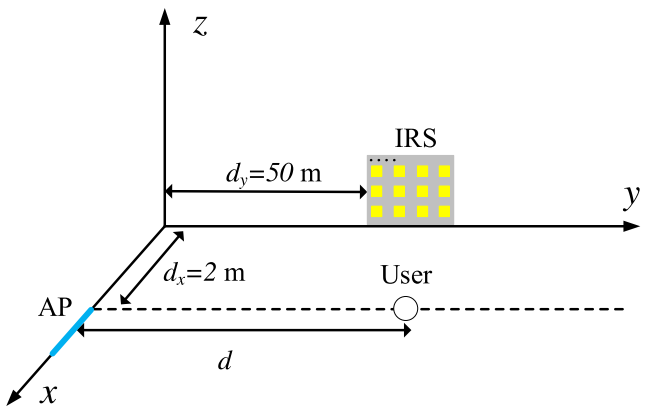

Fig. 2. Simulation setup of the single-user case.

A. Single-User System

1) Performance Comparison With Benchmark Schemes: We consider that one single user lies on a line that is in parallel to y-axis shown in Fig. 2, with its location denoted by $(d_x, d, 0)$. By varying the value of d, the distances of AP-user and IRS-user links change accordingly and we examine the minimum transmit power required for serving the user with a given SNR target. The channel parameters are set as $\alpha_{\mathrm{AI}} = 2.2$, $\alpha_{\mathrm{Iu}} = 2.8$, $\beta_{\mathrm{AI}} = 0$, and $\beta_{\mathrm{Iu}} = \infty$. We compare the following schemes: 1) Lower bound: solve (P1) with $b \to \infty$ or continuous phase shifts by using semidefinite relaxation (SDR) with Gaussian randomization which has been shown to achieve near-optimal performance in [13]; 2) Optimal algorithm: solve problem (23) by using the branch-and-bound method; 3) Successive refinement: use the proposed suboptimal algorithm in Section III-B; 4) Quantization scheme: quantize the continuous phase shifts obtained in 1) to their respective nearest values in $\mathcal{F}$; 5) Codebook based scheme (explained later) which is also used as the phase-shift initialization required in scheme 3); 6) Benchmark scheme without using the IRS by setting $\boldsymbol{w} = \sqrt{\gamma\sigma^2}\boldsymbol{h}_d/\|\boldsymbol{h}_d\|^2$. For schemes 2)-5), we set $b = 1$. For the codebook based scheme, we adopt the widely used Hadamard matrix [44], whose entries are either 1 or -1, thus corresponding to the phase shift of 0 or π. Besides, its columns are mutually orthogonal and thus span the whole N-dimensional space. The codebook based scheme starts by using each of the N columns of the Hadamard matrix as the phase-shift vector $\boldsymbol{\theta}$ and then selects the one resulting in the minimum transmit power at the AP. Note that it generally outperforms the scheme with fixed phase shifts at the IRS since the latter can be considered as a special case of the former with only one single vector in the codebook.

In Fig. 3, we compare the transmit power required at the AP for the above schemes versus the AP-user distance by setting $M = 4$, $N = 16$, and $\gamma = 25$ dB. First, it is observed that the required transmit power of using 1-bit phase shifters is significantly lower than that without the IRS when the user locates in the vicinity of the IRS. This demonstrates

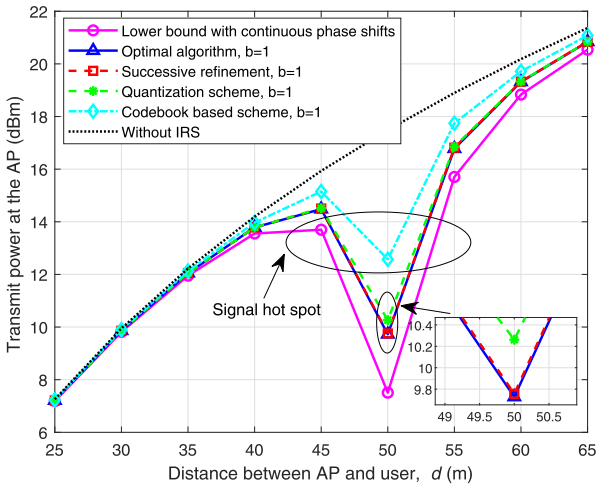

Fig. 3. AP transmit power versus AP-user distance.

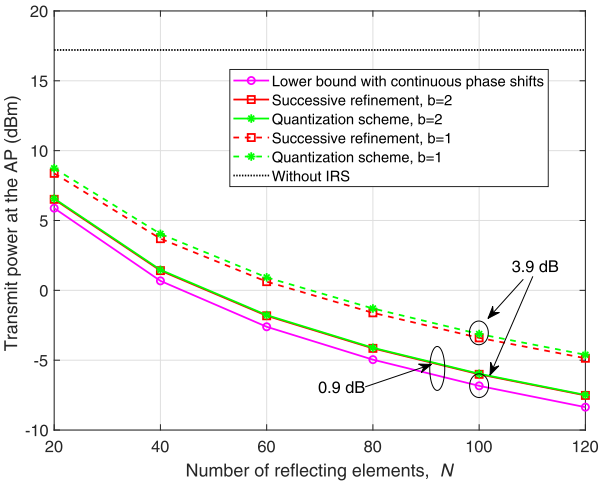

Fig. 4. AP transmit power versus the number of reflecting elements.

the practical usefulness of IRS in creating a "signal hot spot" even with very coarse and low-cost phase shifters. Moreover, one can observe that using the IRS with 1-bit phase shifters suffers performance loss compared to the transmit power lower bound with continuous phase shifts. This is expected since due to discrete phase shifts, the multi-path signals from the AP including those reflected and non-reflected by the IRS cannot be perfectly aligned in phase at the receiver, thus resulting in a performance loss. Finally, it is observed that the proposed successive refinement algorithm and quantization scheme both achieve near-optimal performance in this single-user case, and they significantly outperform the codebook based scheme. This demonstrates the advantage of optimizing phase shifts based on the actual channels over only selecting them from a set of pre-defined phase shift vectors in a codebook.

2) Impact of Discrete Phase Shifts: To validate the theoretical analysis in Proposition 1, we plot in Fig. 4 the AP transmit power versus the number of reflecting elements N at the IRS when $d = 50$ m. In particular, we consider both $b = 1$ and $b = 2$ for discrete phase shifts at the IRS. Other parameters are

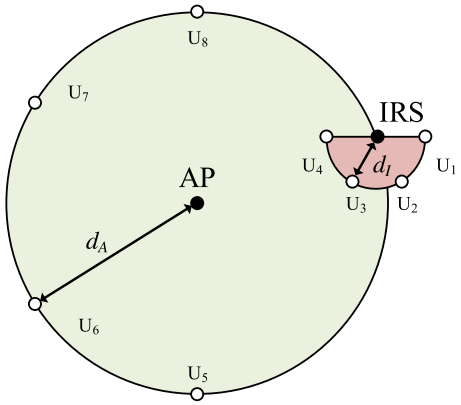

Fig. 5. Simulation setup of the multiuser system (top view) where the deployment of the AP and IRS is the same as that in Fig. 2.

set the same as those in Fig. 3. From Fig. 4, it is observed that as N increases, the performance gap between the quantization scheme (for both $b = 1$ and $b = 2$) and the lower bound (for $b = \infty$) first increases and then approaches a constant that is determined by $\eta(b)$ given in (31) (i.e., $\eta(1) = -3.9$ dB and $\eta(2) = -0.9$ dB shown in Table I). This is expected since when N is moderate, the signal power of the AP-user link is comparable to that of the IRS-user link, thus the misalignment of multi-path signals due to discrete phase shifts becomes more pronounced with increasing N. However, when N is sufficiently large such that the reflected signal power by the IRS dominates in the total received power at the user, the performance loss arising from the phase quantization error converges to that in accordance with the asymptotic analysis given in Proposition 1. In addition, one can observe that in this case the gain achieved by the successive refinement algorithm over the quantization scheme is more evident with $b = 1$ compared to $b = 2$. It is worth pointing out that the quantization scheme needs to first obtain the continuous phase shifts by invoking the semidefinite program (SDP) solver [13] and thus has a higher complexity than the successive refinement algorithm.

B. Multiuser System

Next, we consider a multiuser system with eight users, denoted by U_k's, $k = 1, \cdots, 8$, and their locations are shown in Fig. 5. Specifically, U_k's, $k = 1, 2, 3, 4$, lie evenly on a half-circle centered at the reference element of the IRS with radius $d_I = 2$ m and the rest users lie evenly on a half-circle centered at the reference antenna of the AP with radius $d_A = 50$ m. This setup can practically correspond to the case that the IRS is deployed at the cell-edge to cover an area with a high density of users (e.g., a hot spot scenario). The channel parameters are set as $\alpha_{\rm AI} = 2.2$, $\alpha_{\rm Iu} = 2.8$, $\beta_{\rm AI} = \infty$, and $\beta_{\rm Iu} = 0$. First, we show the convergence behaviour of the proposed successive refinement algorithm in Section IV-B with $M = 8, K = 8, N = 48$, and $\gamma = 15$ dB. As shown in Fig. 6, it is observed that this suboptimal algorithm converges more rapidly for the case of $b = 1$ as compared to that of $b = 2$, while their required complexities are much smaller than that of the optimal exhaustive search, i.e., $\mathcal{O}(2^{bN})$.

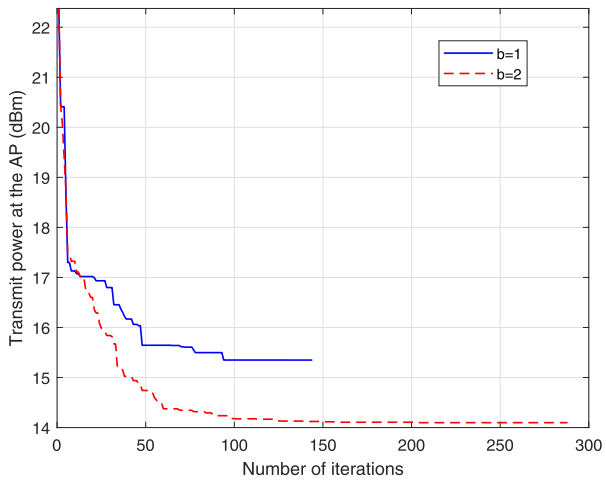

Fig. 6. Convergence behaviour of the ZF-based successive refinement algorithm for the multiuser case with $M = 8, K = 8, N = 48$, and $\gamma = 15$ dB.

1) Performance Comparison With Benchmark Schemes: In Fig. 7, we plot the transmit power versus the user SINR target by setting $b = 1$ under different system setups. We assume that U_k's, $k = 1, 2$, are active (need to be served) for $K = 2$ and U_k's, $k = 1, 2, 3, 4$ are active for $K = 4$. Due to the high complexity of exhaustive search in the optimal algorithm, we consider it as a benchmark scheme only for a relatively small system size shown in Fig. 7(a), while for Figs. 7(b) and 7(c), we propose an MMSE-based successive refinement algorithm as the benchmark. Specifically, in each iteration, we search all the possible values of θ_n over $\mathcal{F}$ by fixing θ_ℓ's, $\forall \ell \neq n, \ell \in \mathcal{N}$, and for each value, we solve (P3) to obtain the MMSE precoder as well as the corresponding AP transmit power. If (P3) is not feasible for a specific phase-shift value in $\mathcal{F}$, the required AP transmit power is set as positive infinity. Then, the phase-shift value that corresponds to the minimum AP transmit power is chosen as the optimal θ_n in each iteration. The above procedure is repeated until the fractional decrease of the objective value is less than the pre-defined threshold. Since the MMSE precoder is the optimal solution to (P3), the transmit power of the MMSE-based successive refinement algorithm generally serves as a lower bound for that of the ZF-based successive refinement algorithm. We compare the following schemes. 1) Optimal algorithm in Section IV-A (for Fig. 7(a) only); 2) MMSE precoding based successive refinement algorithm given above; 3) ZF precoding based successive refinement algorithm proposed in Section IV-B; 4) Quantization scheme: quantizing the continuous phase shifts obtained by using the iterative algorithm in [7] to their respective nearest values in $\mathcal{F}$; 5) Codebook based scheme as in the single-user case; 6) Benchmark scheme without the IRS. For schemes 5) and 6), the MMSE precoder is applied at the AP.

From Figs. 7(a)-7(c), it is first observed that all the algorithms with IRS achieve significant transmit power reduction at the AP as compared to the case without IRS, which demonstrates the effectiveness of IRS in the multiuser scenario. Second, one can observe from Fig. 7(a) that the proposed ZF-based successive refinement algorithm achieves near-optimal performance and outperforms both the quantization and codebook based schemes. In addition, by comparing Figs. 7(a) and 7(c), it is observed that the performance gain of the proposed ZF-based algorithm over benchmark schemes

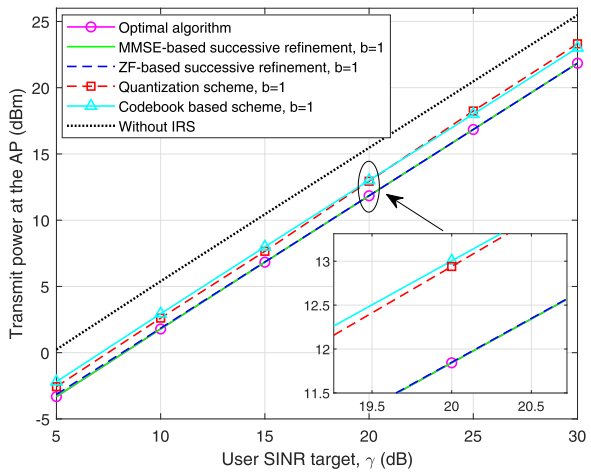

(a) $M = 4, N = 8, K = 2$

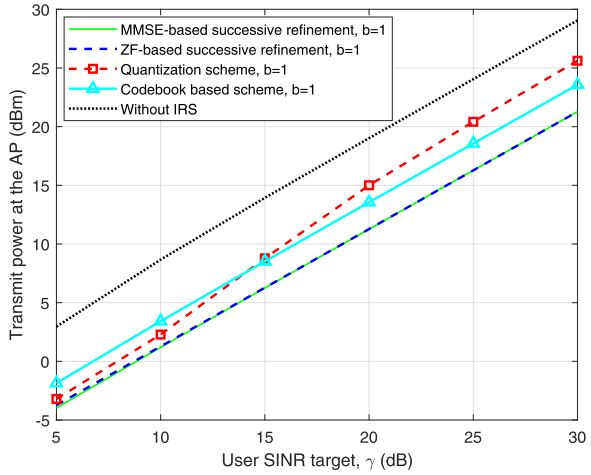

(b) $M = 6, N = 32, K = 4$

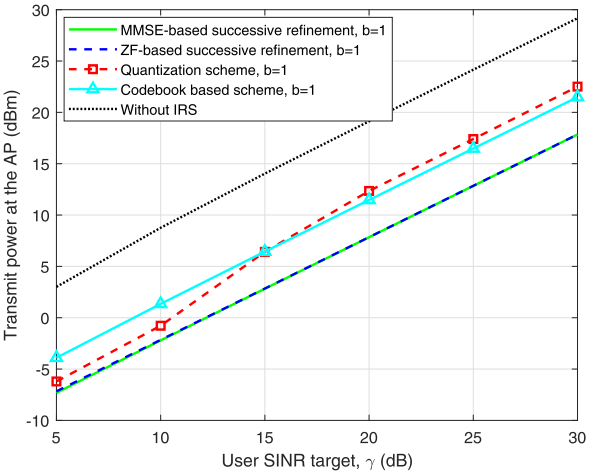

(c) $M = 6, N = 64, K = 4$

Fig. 7. AP transmit power versus the user SINR target under different setups.

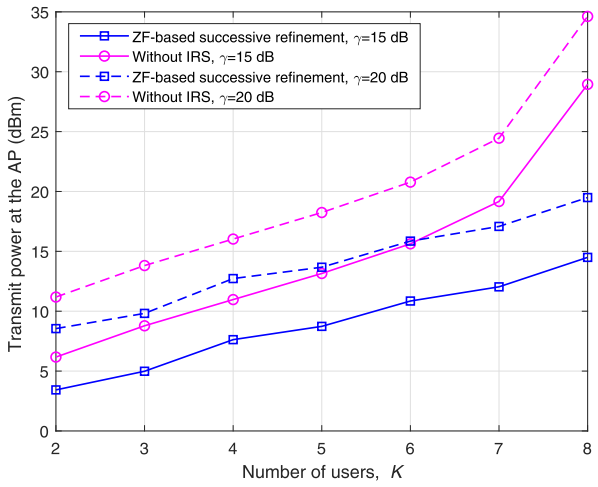

Fig. 8. AP transmit power versus the number of users.

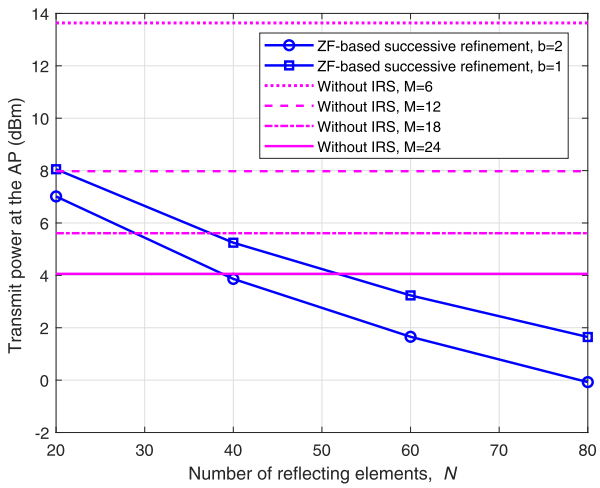

Fig. 9. AP transmit power versus the number of reflecting elements.

becomes more pronounced as the system size becomes larger. This is expected since for the codebook based scheme, the possible combinations of phase-shift vectors grow exponentially as N increases, while the codebook based scheme only linearly increases the codebook size with N. It is worth pointing out that although the quantization scheme suffers from small performance loss in the low SINR regime compared to the proposed ZF-based algorithm, it performs even worse than the codebook based scheme in the high SINR regime, as shown in Figs. 7(a)-7(c). This is because the multiuser interference becomes severe when the user SINR target is high, and thus a coarse quantization from continuous phase shift values to discrete ones results in signal mismatch not only in desired signal combining but also in interference cancellation. Finally, from Figs. 7(a)-7(c), one can observe that the ZF-based algorithm performs almost the same as the MMSE-based algorithm for a wide range of SINR targets in all considered setups. The reason behind such a phenomenon is that the IRS can effectively reduce the undesired channel correlation among users via providing additional controllable multi-path signals to its nearby users.

2) AP Transmit Power Versus Number of Users: In Fig. 8, we show the AP transmit power versus the number of users by setting $M = 8$, $N = 48$, and $b = 1$. All other parameters are the same as those in Fig. 7. In particular, we follow the user index order and successively add one user ($k = 1, 2, 3, 4$) near the IRS and then one user ($k = 5, 6, 7, 8$) far from the IRS to draw useful insights. Note that U_k's, $k = 1, 2, 3, 4$, located in the vicinity of the IRS, have similar path loss as the other U_k's, $k = 5, 6, 7, 8$, in the AP-user links. From Fig. 8, it is first observed that adding a user near the IRS (e.g., adding U_2 corresponds to increasing K from 2 to 3) requires less additional transmit power than that after adding a user far from the IRS (e.g., adding U_6 corresponds to increasing K from 3 to 4), thanks to the passive beamforming gain provided by the IRS. More importantly, one can observe that when the number of users approaches that of antennas at the AP, the transmit power in the case without IRS increases much faster than that in the case with IRS. This further demonstrates that the multiuser interference can be more effectively suppressed by applying the joint active and passive beamforming in the IRS-aided system. Another important implication of the above result is that the IRS has the capability of transforming a *poorly-conditioned* MIMO channel to a *well-conditioned* MIMO channel by adding more controllable multi-paths. For instance, for $K = M = 2$, the multiuser MIMO channel without IRS has a rank approximately given by $\mathrm{rank}(\boldsymbol{H}_d^H) = 1$, if the two users have highly correlated AP-user channels; whereas by leveraging the IRS to actively contribute more signal paths, it is more likely to have $\mathrm{rank}(\boldsymbol{H}_r^H \boldsymbol{\Theta} \boldsymbol{G} + \boldsymbol{H}_d^H) = 2$, thus helping reap the full spatial multiplexing gain in a multiuser MIMO system.

3) IRS-Aided Small MIMO Versus Large MIMO Without IRS: Due to the deployment of IRS, the number of transmit antennas at the AP can be reduced given the same AP transmit power and the users' SINR targets. This thus leads to a potentially more cost-effective solution for future wireless networks by using small MIMO with low-cost IRS as compared to the traditional large (massive) MIMO without the IRS. To compare the performance of these two somewhat opposite design paradigms, we show in Fig. 9 the AP transmit power versus the number of IRS elements with $M = 6$, $\gamma = 15$ dB, and $K = 4$ (i.e., only the four users near the IRS are active). We consider the IRS with $b = 1$ or $b = 2$ as compared to a large MIMO system without using IRS. From Fig. 9, it is observed that for the AP transmit power of 4 dBm, we need to deploy 24 active antennas at the AP in the case without IRS. In contrast, with the same user SINR performance, we can alternatively use a hybrid configuration by deploying only 6 active antennas at the AP together with either 52 1-bit or 38 2-bit passive reflecting elements at the IRS. As a result, the associated RF power consumption and hardware cost for active antennas at the AP are significantly reduced over the case of large MIMO without IRS, thus providing a new cost-effective solution to achieve the same large MIMO performance gain. Therefore, the IRS-aided system provides more flexibility to trade-off between the number of active antennas (M) at the AP and that of passive elements (N) at the IRS as well as their equipped phase shifters with different levels (2^b), to optimally balance between the system performance and cost.

VI. Conclusion

In this paper, we studied the beamforming optimization for IRS-aided wireless communications under practical discrete phase-shift constraints at the IRS. Specifically, the continuous transmit precoder at the AP and discrete phase shifts at the IRS were jointly optimized to minimize the transmit power at the AP while meeting the given user SINR targets. We proposed both optimal and successive refinement based suboptimal solutions for the single-user as well as multiuser cases. Furthermore, we analyzed the performance loss of IRS due to discrete phase shifts as compared to the ideal case with continuous phase shifts, when the number of reflecting elements becomes asymptotically large. Interestingly, it was shown that using IRS with even 1-bit phase shifters is still able to achieve the same asymptotic squared power gain as in the case with continuous phase shifts, subjected to only a constant power loss in dB. Simulation results showed that significant transmit power saving can be achieved by using IRS with discrete phase shifts as compared to the case without IRS, while the performance gains in terms of other metrics such as achievable rate and receive SINR can be similarly shown. In addition, it was revealed that directly quantizing the optimized continuous phase shifts to obtain discrete phase shifts achieves near-optimal performance in the single-user case, while its performance degradation in the multiuser case is non-negligible due to the severe co-channel interference. Finally, it was shown that the ZF precoder based algorithm performs almost as well as the MMSE precoder based algorithm, thanks to the multiuser channel rank improvement with the additional signal paths provided by the IRS.

There are other important issues that are not addressed in this paper yet, some of which are listed as follows to motivate future works.

- Besides phase shifts optimization studied in this paper, the reflection amplitude of IRS's elements can be adjusted to further improve the system performance [6]. However, the joint optimization of reflection amplitude and phase shifts, in the form of either discrete or continuous values, is more challenging to solve. In addition, it is unclear whether the performance gain obtained by such joint phase-amplitude optimization is sufficiently large to justify the increased hardware cost and algorithm complexity in practice, which needs further investigation.
- This paper considered frequency-flat (non-selective) fading channels for narrowband communication. However, when frequency-selective channels are considered, the phase shift design of IRS needs to not only consider the transmit precoder design, but also cater to all signal paths at different delays, due to which the corresponding optimization problem is more challenging to solve. As such, it is worth comparing the IRS-aided small MIMO with the large-scale MIMO in broadband systems.
- In practice, one AP may be assisted by multiple IRSs while each IRS may be deployed to assist more than one APs. Although the local coverage of passive IRSs greatly simplifies the inter-IRS interference management if they are properly separated, the joint user association, transmit precoding, and phase shifts optimization over multiple APs/IRSs is more involved than the single AP/IRS design problem considered in this paper, and thus is worthy of further investigation.
- In the multi-cell scenario, the joint deployment of the active APs and passive IRSs is also an important problem to investigate in future work. For example, the densities of APs and IRSs as well as their locations can be jointly optimized to achieve the desired communication performance at minimum system cost.

References

[1] Q. Wu and R. Zhang, "Beamforming optimization for intelligent reflecting surface with discrete phase shifts," in *Proc. IEEE ICASSP*, May 2019, pp. 7830–7833.

[2] S. Zhang, Q. Wu, S. Xu, and G. Y. Li, "Fundamental green tradeoffs: Progresses, challenges, and impacts on 5G networks," *IEEE Commun. Surveys Tuts.*, vol. 19, no. 1, pp. 33–56, 1st Quart., 2017.

[3] H. Q. Ngo, E. G. Larsson, and T. L. Marzetta, "Energy and spectral efficiency of very large multiuser MIMO systems," *IEEE Trans. Commun.*, vol. 61, no. 4, pp. 1436–1449, Apr. 2013.

[4] Q. Wu, G. Y. Li, W. Chen, D. W. K. Ng, and R. Schober, "An overview of sustainable green 5G networks," *IEEE Wireless Commun.*, vol. 24, no. 4, pp. 72–80, Aug. 2017.

[5] F. Sohrabi and W. Yu, "Hybrid digital and analog beamforming design for large-scale antenna arrays," *IEEE J. Sel. Topics Signal Process.*, vol. 10, no. 3, pp. 501–513, Apr. 2016.

[6] Q. Wu and R. Zhang, "Towards smart and reconfigurable environment: Intelligent reflecting surface aided wireless network," *IEEE Commun. Mag.*, to be published, doi: 10.1109/MCOM.001.1900107.

[7] Q. Wu, and R. Zhang, "Intelligent reflecting surface enhanced wireless network via joint active and passive beamforming," *IEEE Trans. Wireless Commun.*, vol. 18, no. 11, pp. 5394–5409, Nov. 2019.

[8] L. Subrt and P. Pechac, "Intelligent walls as autonomous parts of smart indoor environments," *IET Commun.*, vol. 6, no. 8, pp. 1004–1010, May 2012.

[9] C. Huang, A. Zappone, M. Debbah, and C. Yuen, "Achievable rate maximization by passive intelligent mirrors," in *Proc. IEEE ICASSP*, Apr. 2018, pp. 3714–3718.

[10] C. Huang, A. Zappone, G. C. Alexandropoulos, M. Debbah, and C. Yuen, "Reconfigurable intelligent surfaces for energy efficiency in wireless communication," *IEEE Trans. Wireless Commun.*, vol. 18, no. 8, pp. 4157–4170, Aug. 2019.

[11] X. Tan, Z. Sun, D. Koutsonikolas, and J. M. Jornet, "Enabling indoor mobile millimeter-wave networks based on smart reflect-arrays," in *Proc. IEEE INFOCOM*, Apr. 2018, pp. 270–278.

[12] M. Di Renzo *et al.*, "Smart radio environments empowered by AI reconfigurable meta-surfaces: An idea whose time has come," *EURASIP J. Wireless Commun. Netw.*, to be published.

[13] Q. Wu and R. Zhang, "Intelligent reflecting surface enhanced wireless network: Joint active and passive beamforming design," in *Proc. IEEE GLOBECOM*, Dec. 2018, pp. 1–6.

[14] T. Jiang and Y. Shi, "Over-the-air computation via intelligent reflecting surfaces," 2019, *arXiv:1904.12475*. [Online]. Available: https://arxiv.org/abs/1904.12475

[15] W. Yan, X. Kuai, and X. Yuan, "Passive beamforming and information transfer via large intelligent surface," 2019, *arXiv:1905.01491*. [Online]. Available: https://arxiv.org/abs/1905.01491

[16] X. Yu, D. Xu, and R. Schober, "MISO wireless communication systems via intelligent reflecting surfaces," 2019, *arXiv:1904.12199*. [Online]. Available: https://arxiv.org/abs/1904.12199

[17] M. Cui, G. Zhang, and R. Zhang, "Secure wireless communication via intelligent reflecting surface," *IEEE Wireless Commun. Lett.*, vol. 8, no. 5, pp. 1410–1414, Oct. 2019.

[18] Y. Yang, B. Zheng, S. Zhang, and R. Zhang, "Intelligent reflecting surface meets OFDM: Protocol design and rate maximization," 2019, *arXiv:1906.09956*. [Online]. Available: https://arxiv.org/abs/1906.09956

[19] E. Björnson and L. Sanguinetti, "Demystifying the power scaling law of intelligent reflecting surfaces and metasurfaces," 2019, *arxiv:1908.03133*. [Online]. Available: https://arxiv.org/abs/1908.03133

[20] X. Guan, Q. Wu, and R. Zhang, "Intelligent reflecting surface assisted secrecy communication: Is artificial noise helpful or not?" 2019, *arxiv:1907.12839*. [Online]. Available: https://arxiv.org/abs/1907.12839
[21] J. Chen, Y.-C. Liang, Y. Pei, and H. Guo, "Intelligent reflecting surface: A programmable wireless environment for physical layer security," *IEEE Access*, vol. 7, pp. 82599–82612, 2019.
[22] D. Xu, X. Yu, Y. Sun, D. W. K. Ng, and R. Schober, "Resource allocation for secure IRS-assisted multiuser MISO systems," 2019, *arxiv:1907.03085*. [Online]. Available: https://arxiv.org/abs/1907.03085
[23] Q. Wu and R. Zhang, "Weighted sum power maximization for intelligent reflecting surface aided SWIPT," *IEEE Wireless Commun. Lett.*, to be published, doi: 10.1109/LWC.2019.2961656.
[24] Q. Wu and R. Zhang, "Joint active and passive beamforming optimization for intelligent reflecting surface assisted SWIPT under QoS constraints," *arxiv:1910.06220*. [Online]. Available: https://arxiv.org/abs/1910.06220
[25] C. Pan *et al.*, "Intelligent reflecting surface enhanced MIMO broadcasting for simultaneous wireless information and power transfer," *arxiv:1908.04863*. [Online]. Available: https://arxiv.org/abs/1908.04863
[26] D. Mishra and H. Johansson, "Channel estimation and low-complexity beamforming design for passive intelligent surface assisted MISO wireless energy transfer," in *Proc. IEEE ICASSP*, May 2019, pp. 4659–4663.
[27] M. Fu, Y. Zhou, and Y. Shi, "Intelligent reflecting surface for downlink non-orthogonal multiple access networks," 2019, *arxiv:1906.09434*. [Online]. Available: https://arxiv.org/abs/1906.09434
[28] G. Yang, X. Xu, and Y.-C. Liang, "Intelligent reflecting surface assisted non-orthogonal multiple access," 2019, *arxiv:1907.03133*. [Online]. Available: https://arxiv.org/abs/1907.03133
[29] T. J. Cui, M. Q. Qi, X. Wan, J. Zhao, and Q. Cheng, "Coding metamaterials, digital metamaterials and programmable metamaterials," *Light, Sci. Appl.*, vol. 3, p. e218, Oct. 2014.
[30] N. Kaina, M. Dupré, G. Lerosey, and M. Fink, "Shaping complex microwave fields in reverberating media with binary tunable metasurfaces," *Sci. Rep.*, vol. 4, p. 6693, Oct. 2014.
[31] L. Zhang *et al.*, "Space-time-coding digital metasurfaces," *Nat. Commun.*, vol. 9, no. 1, p. 4334, Oct. 2018.
[32] P. Nayeri, F. Yang, and A. Z. Elsherbeni, *Reflectarray Antennas: Theory, Designs, and Applications*. Hoboken, NJ, USA: Wiley, 2018.
[33] S. Cui, A. J. Goldsmith, and A. Bahai, "Energy-efficiency of MIMO and cooperative MIMO techniques in sensor networks," *IEEE J. Sel. Areas Commun.*, vol. 22, no. 6, pp. 1089–1098, Aug. 2004.
[34] Y. Yang, S. Zhang, and R. Zhang, "IRS-enhanced OFDM: Power allocation and passive array optimization," 2019, *arxiv:1905.00604*. [Online]. Available: https://arxiv.org/abs/1905.00604
[35] C. Huang, B. Sun, W. Pan, J. Cui, X. Wu, and X. Luo, "Dynamical beam manipulation based on 2-bit digitally-controlled coding metasurface," *Sci. Rep.*, vol. 7, Feb. 2017, Art. no. 042302.
[36] B. Zheng and R. Zhang, "Intelligent reflecting surface enhanced OFDM: Channel estimation and reflection optimization," 2019, *arxiv:1909.03272*. [Online]. Available: https://arxiv.org/abs/1909.03272
[37] A. M.-C. So, J. Zhang, and Y. Ye, "On approximating complex quadratic optimization problems via semidefinite programming relaxations," *Math. Program.*, vol. 110, no. 1, pp. 93–110, Jun. 2007.
[38] S. Burer and A. N. Letchford, "Non-convex mixed-integer nonlinear programming: A survey," *Surv. Oper. Res. Manage. Sci.*, vol. 17, no. 2, pp. 97–106, Jun. 2012.
[39] D. Tse and P. Viswanath, *Fundamentals Wireless Communication*. Cambridge, U.K.: Cambridge Univ. Press, 2005.
[40] E. Björnson, J. Hoydis, and L. Sanguinetti, "Massive MIMO networks: Spectral, energy, and hardware efficiency," *Found. Trends Signal Process.*, vol. 11, nos. 3–4, pp. 154–655, Nov. 2017.
[41] A. Wiesel, Y. C. Eldar, and S. Shamai, "Linear precoding via conic optimization for fixed MIMO receivers," *IEEE Trans. Signal Process.*, vol. 54, no. 1, pp. 161–176, Jan. 2006.
[42] M. Schubert and H. Boche, "Solution of the multiuser downlink beamforming problem with individual SINR constraints," *IEEE Trans. Veh. Technol.*, vol. 53, no. 1, pp. 18–28, Jan. 2004.
[43] Z.-Q. Luo and W. Yu, "An introduction to convex optimization for communications and signal processing," *IEEE J. Sel. Areas Commun.*, vol. 24, no. 8, pp. 1426–1438, Aug. 2006.
[44] X. Liu, W. Zou, and S. Chen, "Joint design of analog and digital codebooks for hybrid precoding in millimeter wave massive MIMO systems," *IEEE Access*, vol. 6, pp. 69818–69825, 2018.

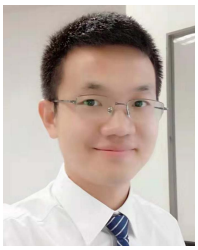

Qingqing Wu (S'13–M'16) received the B.Eng. degree in electronic engineering from the South China University of Technology in 2012 and the Ph.D. degree in electronic engineering Shanghai Jiao Tong University (SJTU) in 2016. He is currently a Research Fellow with the Department of Electrical and Computer Engineering, National University of Singapore. His current research interest includes intelligent reflecting surface (IRS), unmanned aerial vehicle (UAV) communications, and green communications. He was a recipient of the Outstanding Ph.D. Thesis Funding in SJTU in 2016 and the Outstanding Ph.D. Thesis Award of China Institute of Communications in 2017. He received the IEEE WCSP Best Paper Award in 2015, the Exemplary Reviewer Award of IEEE COMMUNICATIONS LETTERS in 2016 and 2017, IEEE WIRELESS COMMUNICATIONS LETTERS in 2018, IEEE TRANSACTIONS ON COMMUNICATIONS in 2017 and 2018, and IEEE TRANSACTIONS ON WIRELESS COMMUNICATIONS in 2017 and 2018. He serves as an Associate Editor of IEEE COMMUNICATIONS LETTERS and IEEE OPEN JOURNAL OF THE COMMUNICATIONS SOCIETY, a Guest Editor of IEEE OPEN JOURNAL OF VEHICULAR TECHNOLOGY on 6G Intelligent Communications, and a Leading Guest Editor of IEEE JOURNAL ON SELECTED AREAS IN COMMUNICATIONS on UAV Communications in 5G and Beyond Networks. He is the workshop Co-Chair of ICC 2019 and ICC 2020 workshop on Integrating UAVs into 5G and Beyond.

Rui Zhang (S'00–M'07–SM'15–F'17) received the B.Eng. degree (Hons.) and the M.Eng. degree from the National University of Singapore, Singapore, and the Ph.D. degree from Stanford University, Stanford, CA, USA, all in electrical engineering.

From 2007 to 2010, he worked with the Institute for Infocomm Research, ASTAR, Singapore. Since 2010, he has been working with the National University of Singapore, where he is currently a Professor with the Department of Electrical and Computer Engineering. He has published more than 200 journal articles and more than 180 conference papers. He has also been listed as a Highly Cited Researcher by Thomson Reuters/Clarivate Analytics, since 2015. His current research interests include UAV/satellite communications, wireless power transfer, reconfigurable MIMO, and optimization methods.

Dr. Zhang serves as a member of the Steering Committee of IEEE WIRELESS COMMUNICATIONS LETTERS. He was a recipient of the 6th IEEE Communications Society Asia-Pacific Region Best Young Researcher Award in 2011, and the Young Researcher Award of National University of Singapore in 2015. He was a co-recipient of the IEEE Marconi Prize Paper Award in Wireless Communications in 2015, IEEE Communications Society Asia-Pacific Region Best Paper Award in 2016, IEEE Signal Processing Society Best Paper Award in 2016, IEEE Communications Society Heinrich Hertz Prize Paper Award in 2017, IEEE Signal Processing Society Donald G. Fink Overview Paper Award in 2017, and IEEE Technical Committee on Green Communications and Computing (TCGCC) Best Journal Paper Award in 2017. His coauthored article received the IEEE Signal Processing Society Young Author Best Paper Award in 2017. He served for more than 30 international conferences as the TPC Co-Chair or an Organizing Committee Member, and as the Guest Editor for three special issues in IEEE JOURNAL OF SELECTED TOPICS IN SIGNAL PROCESSING and IEEE JOURNAL ON SELECTED AREAS IN COMMUNICATIONS. He was an elected member of IEEE Signal Processing Society SPCOM Technical Committee from 2012 to 2017 and a SAM Technical Committee from 2013 to 2015, and served as the Vice Chair of IEEE Communications Society Asia-Pacific Board Technical Affairs Committee from 2014 to 2015. He served as an Editor for IEEE TRANSACTIONS ON WIRELESS COMMUNICATIONS from 2012 to 2016, IEEE JOURNAL ON SELECTED AREAS IN COMMUNICATIONS: Green Communications and Networking Series from 2015 to 2016, and IEEE TRANSACTIONS ON SIGNAL PROCESSING from 2013 to 2017. He is currently an Editor of IEEE TRANSACTIONS ON COMMUNICATIONS and IEEE TRANSACTIONS ON GREEN COMMUNICATIONS AND NETWORKING. He is also a Distinguished Lecturer of IEEE Signal Processing Society and IEEE Communications Society.